Journal of Controlled Release 251 (2017) 37–48

Contents lists available at ScienceDirect

Journal of Controlled Release

journal homepage: www.elsevier.com/locate/jconrel

Differentially cleaving peptides as a strategy for controlled drug release in human retinal pigment epithelial cells

Madhushree Bhattacharya [a,*], Sanjay Sarkhel [a], Jonne Peltoniemi [a], Robert Broadbridge [b], Marjo Tuomainen [c], Seppo Auriola [c], Arto Urtti [a,c]

[a] Centre for Drug Research, Division of Pharmaceutical Biosciences, University of Helsinki, Helsinki, Finland
[b] Peptide Protein Research Ltd, Hampshire, England, United Kingdom
[c] School of Pharmacy, University of Eastern Finland, Kuopio, Finland

ARTICLE INFO

Article history:
Received 15 November 2016
Received in revised form 10 February 2017
Accepted 13 February 2017
Available online 16 February 2017

Keywords:
Drug delivery
Ocular therapeutics
Retina
Retinal pigment epithelium
Drug targeting
Peptide
Conjugation

ABSTRACT

Currently, drug delivery to the posterior eye segment relies on intravitreal injections of therapeutics. This approach requires frequent injections and does not guarantee drug delivery to intracellular targets. Controlled release systems and nanoparticles are being investigated to mitigate these challenges but most of these approaches lack translational success to the clinics. In our present study, we report a peptide-based delivery system that utilizes enzyme assisted cleavable linkers to release conjugated cargo within the retinal pigment epithelial (RPE) cells. Peptide linkers with differential cleavage rates were developed and tested in the vitreous humor, RPE cell homogenates and intact RPE cells. Selected peptide linkers were conjugated to cell penetrating peptides and D-peptide cargoes. The peptide-based delivery systems were non-toxic to the RPE cells, chemically stable in porcine vitreous and delivered cargo prototypes (hydrophobic & hydrophilic) to the RPE cells. Importantly, we show quantitatively with LC/MS analytics that the intracellular cargo release is controlled by the sequence of the peptide linker. The controlled cleavage of the peptide linkers is not only a useful strategy for intracellular drug delivery to the RPE targets but might also be useful in utilizing the RPE cells as mediators of drug delivery to intracellular targets and surrounding tissues (such as neural retina and choroid).

1. Introduction

Drug delivery to the posterior segment of the eye is a major challenge. This is due to the unique anatomy and physiological barriers in the eye. Topical eye drop administration does not deliver adequate drug concentrations to the retina whereas systemic administration is hampered by the blood retina-barrier [1]. For these reasons, invasive intravitreal injections are commonly used to deliver Fab-fragments, IgG based antibodies, corticosteroids and soluble receptors in the treatment of the posterior segment of the eye [2–5]. Sub-conjunctival, suprachoroidal, and periocular routes have been proposed as alternatives to intravitreal injections [6–9], but these approaches do not result in effective retinal drug delivery [10]. In the case of the sub-retinal route, the technique is too demanding for wide clinical use [11].

New retinal therapeutics are being widely explored as most retinal diseases are still without effective treatment. Retinal drug discovery includes small molecular drugs, proteins and nucleotide-based gene products. In many cases, the drug targets are located in intracellular compartments [12,13]. For example, pathological changes (protein aggregation, oxidative stress, inflammation) take place within the retinal pigment epithelial cells in diseases such as the dry form of age-related macular degeneration [14–16]. Unfortunately, most nucleotide and peptide-based compounds have poor permeability into the target cells [17,18]. Intracellular drug delivery systems are needed for the development of effective retinal treatments. Nanoparticle based formulations, such as liposomes and polymeric nanoparticles have been used to augment the intracellular delivery of biologicals [19–21] but intracellular drug release from particulate based systems is often poorly controlled [12,22]. Furthermore, access of the nanoparticles to target cell layers in the retina is also problematic, especially in the case of cationic nanoparticles that are usually used for intracellular delivery of DNA and RNA based drugs [23]. These formulations tend to stick to the vitreous or inner limiting membrane of the retina [24,25].

The major challenges in the retinal drug delivery are (a) prolongation of the intravitreal dosing interval; (b) intracellular delivery of peptide and nucleotide based drugs (e.g. oligonucleotides, proteins); (c) replacement of intravitreal injections with less invasive modes of drug delivery. Clinical VEGF-A antagonists (treatment of wet AMD) such as IgG antibodies (bevacizumab), Fab-fragment (ranibizumab), and soluble VEGF receptor (aflibercept) [26–28] are injected intravitreally once a month or bi-monthly. Most other drugs (e.g. small molecules) cannot

* Corresponding author.
E-mail address: madhushree.bhattacharya@helsinki.fi (M. Bhattacharya).

http://dx.doi.org/10.1016/j.jconrel.2017.02.013
0168-3659/

be given as intravitreal injections because they are rapidly eliminated from the posterior eye segment necessitating injections at too short intervals to be clinically feasible [29]. To mitigate such issues, controlled drug delivery systems are very much desired for intravitreal treatments. Currently investigated systems include polymeric implants, microspheres and encapsulated cells [30–33]. Intravitreal delivery of implants and microspheres is invasive and material toxicity hampers the development of many systems [34]. Furthermore, these systems lack the inherent ability to deliver the cargo into the target cells.

We aimed to generate a peptide-based drug delivery system that is based on adequate intracellular access and controlled cargo release within the RPE cells. The delivery system is intended for intravitreal administration. Other possible routes of delivery could be suprachoroidal and periocular. Furthering on the idea of using endogenous components to trigger intracellular release, we have explored enzyme-assisted 'peptide-based cleavable linkers' (PCLs) to control cargo release within the RPE cells. Cathepsin D, a lysosomal enzyme, has relatively high expression levels in RPE cells [35]. Consequently, peptide sequences sensitive to cathepsin D were selected as PCLs. The *N*-terminus of the PCLs was conjugated with cell penetrating peptides (CPPs) and D-pentapeptide cargoes were conjugated at the *C*-terminus. CPPs are charged peptide sequences capable of intracellular delivery of molecular cargo [36,37]. D-Pentapeptide cargoes were chosen for ease of synthesis, resistance to proteolytic cleavage, convenient detection and easy manipulation of the sequence to modify physicochemical properties of the cargo prototypes (hydrophobic/hydrophilic). Controlled drug delivery from the intracellular depots was demonstrated and quantitated with LC/MS. The design and strategy of the approach are depicted in Scheme 1.

2. Materials and methods

2.1. Peptide synthesis

All the PCLs containing both natural and unnatural amino acids (Tables 1, 3); CPP-PCL chimeras (Scheme 2); cargo conjugates (CCs, Table 2) and labeled cargo fragments (Table 2) used in this study were synthesized by Peptide Synthetics-Peptide Protein Research Ltd. (Hampshire, UK). In general, the peptides were synthesized using solid phase peptide synthesis via standard Fmoc chemistry [38] in a 0.1 mmol scale using a Symphony automated peptide synthesizer (Protein Technologies, Arizona). Internally quenched oligopeptide sequences (Scheme 3) contained the fluorescence resonance energy (FRET) pair EDANS/Dabcyl (DABCYL: 4-{[4-(dimethyl amino) phenyl] azo} benzoic acid; EDANS: 5-[(2-aminoethyl) amino] naphthalene-1-sulfonic acid). Spectral properties of EDANS/Dabcyl are shown in Fig. S1 (Supplementary material). For FRET, the donor and acceptor moieties must be in close proximity, typically 10–100 Å. The typical förster radius (R_0) value for EDANS/Dabcyl pair is 33 Å [39]. Considering the axial distance between the alpha carbon atoms of two adjacent residues to be about 3.5 Å; EDANS and Dabcyl moieties were placed 10–13 residues apart in all the oligopeptides (PCLs: Table 1; PCL analogs: Table 3; CPP-PCL chimeras: Scheme 2). The peptides were purified via Prep RP-HPLC using a Varian system comprising of two 210 pumps, a 320 UV dual wavelength detector and Varian star software employing gradients between the mobile phases, water (0.1% TFA) and acetonitrile (0.1% TFA); equipped with a C18 Gemini Axia column (5 μm particle size, 110 Å pore size, 200 mm by 21 mm, Phenomenex). Fractions containing the desired peptide as indicated by UV absorbance were collected manually; analyzed by LC-MS (Agilent 1100 systems equipped with Aeris core shell column, 100A 150 × 4.6 mm) to determine the purity and freeze dried.

2.2. FRET-based peptide cleavage assay

An assay to determine the cleavage rates of the synthesized oligopeptides with FRET pair EDANS/Dabcyl was carried out using either purified enzyme (cathepsin D) or ARPE-19 cell lysate at oligopeptide concentration of 20 μM. The assay was performed in 96-well black plates in 0.1 M sodium acetate buffer pH 4.0 (100 μl). Briefly, ARPE-19 cells were lysed using lysis buffer (Biovision, California, USA) and lysates were centrifuged at 10,000*g* for 10 min at 4 °C and the supernatant was used for the enzymatic assay. Oligopeptide sequences containing the FRET pair were mixed with cell lysate supernatant and the reaction mixture was incubated at 37 °C. The substrate cleavage was monitored by measuring the fluorescence as a function of time (excitation 340 nm; emission 490 nm) using a microplate fluorescence reader (Varioskan Flash, Thermo Scientific). 100% cleavage was assessed based on the fluorescence obtained from an equimolar free concentration of EDANS (the chromophore present in oligopeptides).

2.3. Cell culture

ARPE-19 cells (human retinal pigment epithelial cell line, ATCC CRL-2302) were cultured in Dulbecco's Modified Eagle Medium: Nutrient Mixture F-12 (DMEM/F-12) supplemented with 10% fetal bovine serum (Gibco), 100 U/ml penicillin, 100 μg/ml streptomycin and 2 mM L-glutamine (Gibco). The cells were cultured in a T-75 flask at 37 °C in a

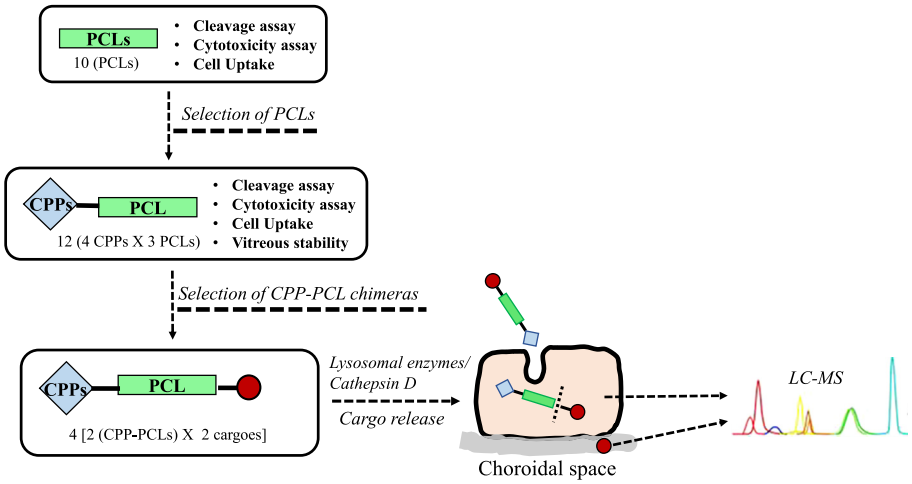

Scheme 1. Overview of design and experimental set up of the peptide based cargo delivery system.

Table 1
Peptide based cleavable linkers (PCLs) screened for cathepsin D enzymatic assay.

	PCL sequences[a]													
	P8	P7	P6	P5	P4	P3	P2	P1	P1′	P2′	P3′	P4′	P5′	P6′	P7′
PCL1		K*	G	K	P	I	L	F	F	R	L	K	r	E*	
PCL2	K**	G	S	K	P	I	L	F	F	R	L	K	r	E*	
PCL3	K*	G	S	K	P	I	L	F	F	R	L	K	r	E*	
PCL4				K**	P	I	L	F	F	R	L	G	K	E*	
PCL5				K*	P	I	L	F	F	R	L	G	K	E*	
PCL6		K**	G	S	P	I	L	F	F	R	L	G	K	E*	
PCL7		K**	G	S	P	I	L	F	F(4NO$_2$)	R	L	E*			
PCL8		K**	G	S	P	I	V	F	F(4NO$_2$)	R	L	E*			
PCL9			K**	G	S	K	N	L	I	P	R	L	E*		
PCL10				K**	G	S	A	L	I	S	W	I	K	R	E*

E* refers to fluorescence donor EDANS (5-[(2-aminoethyl) amino] naphthalene-1-sulfonic acid) attached to glutamic acid side chain.
K* and K** denotes fluorescence quencher Dabcyl (4-{[4-(dimethyl amino) phenyl] azo} benzoic acid) amidated to lysine side chain and the *N*-terminus, respectively. All peptides were synthesized as carboxamide ($CONH_2$) at the *C*-terminus.
[a] Lower case single letter amino acid abbreviation denotes D-amino acid.

7% CO_2 atmosphere. The cells were sub-cultured once a week until they reached 80% confluency. The culture media were changed twice a week.

To obtain polarized and differentiated RPE cells (blood-retina-barrier model), ARPE-19 cells were cultured on Transwell filters as described earlier [40]. Briefly, cells were seeded at a density of 1.6×10^5 cells/cm^2 on laminin coated Transwell permeable supports (surface area 4.67 cm^2, pore size 0.4 μm, Corning Life Sciences, Corning, NY, USA) and differentiated for 4 weeks. The basic filter culture medium (also referred to as basic filter medium) contained only 1% FBS but was otherwise same as above. The cells were maintained at 37 °C in 7% CO_2 atmosphere. Trans-epithelial electrical resistance (TER) of the ARPE monolayer was measured by Endohm™ starting from the second week of Transwell culture. Cell passages from 28 to 34 were used.

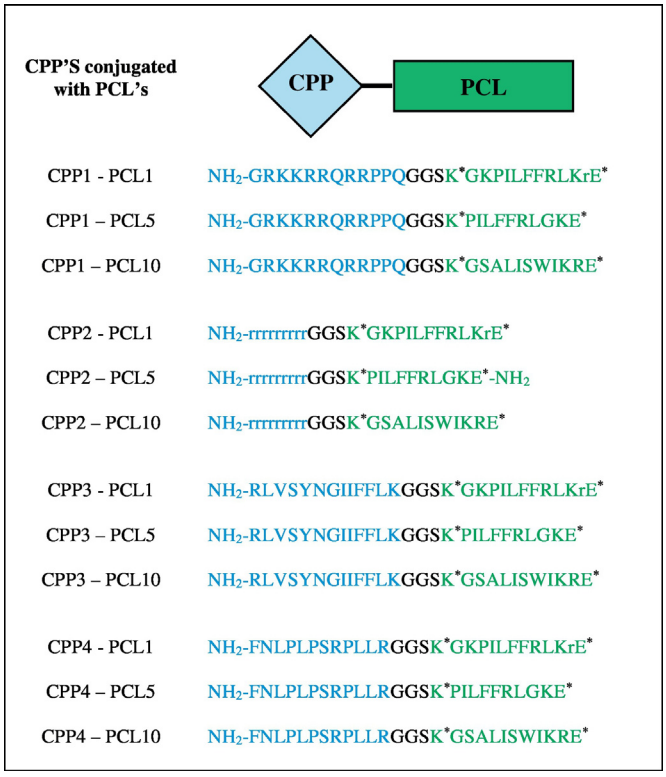

Scheme 2. CPPs conjugated with PCLs. [a]Lower case single letter amino acid abbreviation refers to D-amino acid. E* denotes fluorescence donor EDANS (5-[(2-aminoethyl) amino] naphthalene-1-sulfonic acid) attached to the glutamic acid side chain and K* refers to Dabcyl (4-{[4-(dimethyl amino) phenyl] azo} benzoic acid) amidated to the lysine side chain.

2.4. Cytotoxicity assay

Cytotoxicity of the oligopeptide constructs was evaluated using MTT assay. In this method, NADPH-dependent cellular oxidoreductase enzyme reduces the tetrazolium dye MTT 3-(4, 5-dimethylthiazol-2-yl)-2, 5-diphenyltetrazolium bromide to insoluble formazan in the mitochondria of living cells. The assay was performed as previously described [41]. Briefly, the cells were seeded in 96-well plates at a density of 20,000 cells per well in 150 μl growth medium. After overnight incubation, the cells were washed with PBS. Peptides at various concentrations (0.032–100 μM) in complete cell growth medium (100 μl) were added to each well for incubation (5 h at 37 °C; 5% CO_2). Poly-L-Lysine (PLL) treated and untreated cells served as negative and positive control respectively. After incubation, the media containing peptides was aspirated, the wells were washed with PBS and 150 μl of growth medium was added to the cells. Then, after 24 h incubation, the cells were washed with PBS. A mixture of 90 μl of complete growth media and 10 μl of 5 mg/ml of MTT solution was added to all the wells. The plates were incubated for 4 h at 37 °C. After incubation, 100 μl of 10% sodium dodecyl sulfate (Merck) in 0.01 M HCl (Sigma-Aldrich) was added to the wells to solubilize formazan crystals followed by overnight incubation at 37 °C. Formazan was quantified by measuring absorbance at 570 nm using a spectral scanning multimode plate reader (Varioskan Flash, Thermo Scientific). Cell viability of the treated cells was compared to the untreated control cells.

2.5. Cell uptake studies

Cellular uptake of oligopeptide constructs was determined by flow cytometry. One day before the experiment, ARPE-19 cells were seeded in 6-well plates at a density of 400,000 cells/well in 2 ml growth medium. Prior to the uptake studies, the cells were rinsed twice with 2 ml HBSS buffer (Gibco, supplemented with 10 mM Hepes, pH 7.4) and equilibrated in the same buffer for 30 min at 37 °C. The cells were then treated with FRET pair containing oligopeptide constructs (5 μM) for 1 h at 37 °C. After washing the cultures thrice with 2 ml HBSS buffer (containing 10 mM Hepes pH 7.4), the cells were detached from the wells using 0.25% trypsin/EDTA (Tryplex®). The cells were harvested and centrifuged at 1000 rpm for 5 min, and the cell pellet was gently suspended in 1 ml HBSS buffer, transferred to FACS tubes and immediately analyzed by flow cytometry (BD FACS Aria II Cell sorter) with a near UV laser (375 nm) as the excitation source. Fluorescence of EDANS was recorded with a 450/20 band-pass filter. For each sample, 10,000 events were collected. Each experiment was performed in triplicate. Control cells without exposure to the oligopeptides were visualized on a forward angle light scatter (FSC) versus a 90° angle side scatter (SSC) display. The major cell population was gated and only

Table 2
Cargo conjugates (CCs) and corresponding fragments after intracellular cleavage. Fragments were detected by LC-MS. The CPP, PCL and cargo sequences are shown in blue, green and red, respectively. A short flexible linker (Gly-Gly-Ser), shown in black, was introduced in between the CPP and PCL sequences.

Cargo conjugate #	Sequence of cargo conjugates[a]	Fragment detected	Fragment mass	
			Calc.	Detected (MH^{+1} mono)
CC-1	KGKPILFFRLKr-fwpVl	rfwpVl-NH_2	815.4	816.4
		KrfwpVl-NH_2	943.5	944.5
CC-2	KGKPILFFRLKr-ynaVl	rynaVl-NH_2	733.4	734.4
		KrynaVl-NH_2	861.5	862.5
CC-3	GRKKRRQRRPPQGGSKGKPILFFRLKr-fwpVl	rfwpVl-NH_2	815.4	816.4
		KrfwpVl-NH_2	943.5	944.5
CC-4	GRKKRRQRRPPQGGSKGKPILFFRLKr-ynaVl	rynaVl-NH_2	733.4	734.4
		KrynaVl-NH_2	861.5	862.5
CC-5	GRKKRRQRRPPQGGSKGSALISWIKR-fwpVl	rfwpVl-NH_2	815.4	816.4
		KrfwpVl-NH_2	943.5	944.5
CC-6	GRKKRRQRRPPQGGSKGSALISWIKR-ynaVl	rynaVl-NH_2	733.4	734.4
		KrynaVl-NH_2	861.5	862.5

For interpretation of the references to colour in this table note, the reader is referred to the web version of this article.
[a]Lower case single letter amino acid abbreviation refers to D-amino acid. All CCs were synthesized as acetylation at the *N*-terminal and carboxamide ($CONH_2$) at the *C*-terminus.

the cells falling within this area were used for further analysis. Data was analyzed using FACS Diva version 6.1.3 (BD).

2.6. In vitro stability of oligopeptides in porcine vitreous

Stability of the oligopeptides against enzymatic degradation in porcine vitreous was determined. Porcine eyes were procured from a local slaughterhouse. The eyes were kept on ice bath during the isolation of vitreous humor. The eyes were first cleaned of extra-ocular material and dipped in 70% ethanol. Then, the eyes were opened by incision with a dissecting knife and the clear vitreous humor was separated gently from neural retina. Isolated vitreous humor was homogenized, centrifuged (3200*g*) for 1 h at +4 °C and the supernatant was sterile-filtered using a 0.22 μm filter to remove cellular debris and microbial contamination. The vitreous was stored at −80 °C. For stability studies, oligopeptides with FRET pair were added to the porcine vitreous humor in a 96 well black plate. The mixture was incubated at 37 °C and the cleavage of the oligopeptide was monitored by measuring the EDANS fluorescence as a function of time (excitation 340 nm; emission 490 nm) using a microplate fluorescence reader (Varioskan Flash, Thermo Scientific).

2.7. Quantitative cargo release in the RPE cells

Two D-pentapeptide sequences, fwpVl (log D = +2.0) and ynaVl (log D = −2.0) were chosen as cargoes that are prototypes of small molecular hydrophobic and hydrophilic drugs, respectively (Table 2). The cargoes were conjugated to the *C*-terminal of CPP-PCL chimeras.

Firstly, cargo release was estimated using sub-confluent ARPE-19 cells that were cultured on wells. Experiments were performed 48 h after seeding of the ARPE-19 cells on 6-well plates at a density of 500,000 cells/well. At that time the cells achieved a sub-confluent monolayer (approximately 80–90% confluence). Prior to the experiment, the cells were rinsed twice with PBS (Gibco). Cargo containing oligopeptide solutions were freshly prepared in complete growth medium (DMEM/F-12; supplemented with 100 U/ml streptomycin/penicillin and 2 mM L-glutamine). The cells were then incubated with the oligopeptides (5 μM/well) for 1 h at 37 °C. Subsequently, the cells were washed three times with PBS and detached from the bottom of the wells with TrypLE Express Enzyme (Gibco). The number of cells harvested from each well was determined. The cells were lysed by addition of cell lysis buffer (Biovision) following the manufacturer's instructions. Clear cell lysate obtained from each well was transferred into low binding eppendorf tubes (Eppendorf®) and stored on ice before LC-MS analyses.

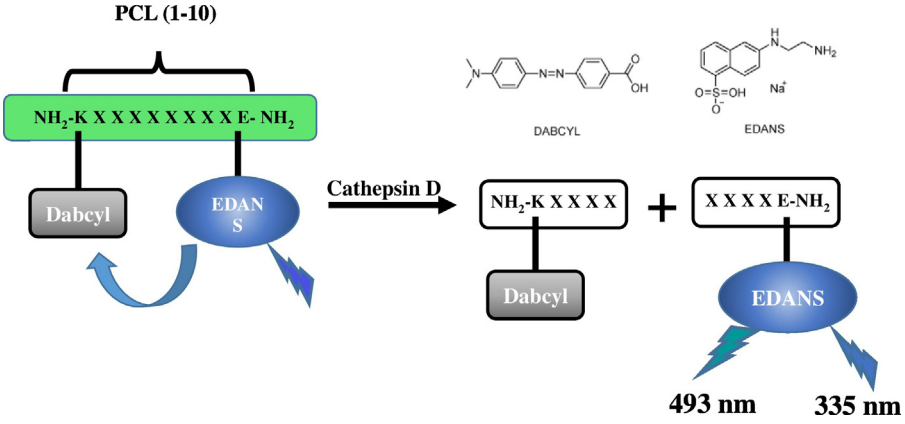

Scheme 3. FRET based screening assay with EDANS/Dabcyl as the donor/acceptor pair. Fluorescence is detected upon cleavage of the peptide scissile bond by the enzyme, cathepsin D.

Table 3
Sequences of PCL analogs.

	P7	P6	P5	P4	P3	P2	P1	P1′	P2′	P3′	P4′	P5′	P6′	P7′
PCL1-a	K*	G	K	P	I	L	F	F	R	L	K	**Cit**	E*	
PCL1-b	K*	G	K	P	I	L	**1-Nal**	**1-Nal**	R	L	K	r	E*	
PCL1-c	K*	G	K	P	I	L	**W**	**W**	R	L	K	**R**	E*	
PCL8-a	K**	G	S	P	I	V	F	F($4NO_2$)	R	L	E	**R**	E*	
PCL10-a			K**	G	S	A	**F**	**F**	S	W	I	K	R	E*
PCL10-b			K**	G	S	A	L	I	S	**Chg**	I	K	R	E*
PCL10-c			K**	G	S	A	L	I	S	W	I	K	E*	
PCL10-d			K**	G	S	**Aib**	L	I	S	W	I	K	R	E*
PCL10-e			K**	G	S	**G**	L	I	S	W	I	K	R	E*
PCL10-f			K**	G	S	A	L	I	**Me-S**	W	I	K	R	E*

E* refers to fluorescence donor EDANS (5-[(2-aminoethyl) amino] naphthalene-1-sulfonic acid) attached to glutamic acid side chain.
K* and K** denotes fluorescence quencher Dabcyl (4-{[4-(dimethyl amino) phenyl] azo} benzoic acid) amidated to lysine side chain and the *N*-terminus, respectively.
All peptides were synthesized as carboxamide ($CONH_2$) at the *C*-terminus. The natural and unnatural amino acid substitutions in the parent PCL's are denoted in bold. Cit = L-Citrulline, 1-Nal = L-1-Naphthylalanine, F($4NO_2$) = 4-Nitro-L-phenylalanine, Chg = L-cyclohexylglycine, Aib = 2-Aminoisobutyric acid, Me-S = 2-Methyl-L-serine.
[a] D-Amino acid is denoted in lower case.

Secondly, cargo release was estimated using polarized differentiated ARPE-19 cells that were cultured on the filters. ARPE-19 cells were cultured as a monolayer on Transwell filters for four weeks to obtain polarized and differentiated cells as described earlier [40]. The medium was replaced on both the apical and basolateral compartments twice a week. After four weeks of culture, the cells were treated with the cargo containing oligopeptides (5 μM) on the apical side for 1 h (7% CO_2, 37 °C). Subsequently, the medium was removed from both the apical and basolateral compartments and the cells were washed three times with PBS. Fresh complete growth medium was added to both the apical and basolateral compartments. The zero-time point sample was collected immediately from the basolateral compartment and the cell culture was continued. Thereafter, samples were collected from the basolateral compartment at time intervals (8 h, 24 h, 48 h and 72 h) and after each sampling, an equivalent amount of fresh medium was added to the basolateral compartment. Samples were stored in low binding Eppendorf tubes at 4 °C.

2.8. LC-MS analysis

To identify cargo fragments released in the cells (cell lysate) and by passive diffusion (basolateral compartment) Section 2.7, three volumes of cold acetonitrile were added to each sample, vortexed and stored at room temperature for 1 h. The samples were centrifuged for 10 min at 12,000*g* to remove precipitates. The supernatant was freeze-dried and stored at −20 °C for further LC-MS analysis.

For quantitative analysis, cargo peptide fragments with isotope labeled amino acid were used as internal standards (Table 2). The L-valine residue in the cargo peptide fragment was labeled for this purpose and the internal standards were calibrated. The cargo peptide fragments were quantified by comparing the peak area to that of the internal standards. For this, samples from the cell lysate and the basolateral compartment were spiked with the internal standards before adding the extraction solvent. Three volumes of cold acetonitrile were added to each spiked sample, vortexed and kept at room temperature for 1 h. The samples were centrifuged for 10 min at 12,000*g* to remove any precipitates. The supernatant was freeze-dried and stored at −20 °C for further LC-MS analysis.

LC-MS analysis was performed on an Agilent 1290 UPLC system connected to Agilent 6540 Q-TOF mass spectrometer (Agilent, Waldbronn, Germany). The instrument was used in positive electrospray ionization and full scan mode. Prior to the LC-MS analysis, the samples were dissolved in 150 μl of 10% ACN containing 0.5% formic acid. Injection volume was 2 μl and the mobile phases were delivered at a flow rate of 0.4 mL/min using the gradient: 5%–70% ACN on a Kinetex 2.6 μm C18, 100 × 2.1 mm column (Phenomenex, Torrance, CA, USA).

The extracted ion chromatogram (EIC) for each peptide fragments obtained from the LC-QTOF/MS run was analyzed using Agilent Mass Hunter Qualitative Analysis software (Santa Clara, California, USA). Each peptide fragment was analyzed using 20 ppm mass window and peak areas on channels with 2, 3 and 4 monoisotopic charges were summed. Sequences of analyzed peptides, their exact masses and ions used for quantitation are listed in Table 2. The exact masses of the cargo conjugates and the corresponding fragments were calculated using UCSF MS-product program (http://prospector.ucsf.edu).

2.9. Computational modeling of cathepsin D - PCL complexes

Structural models of PCL binding to cathepsin D were obtained using the de novo prediction tool PEP-FOLD3 [42]. Briefly, the enzyme-peptide complexes were generated starting from defining a patch of the interaction site(s). For the native substrate (PCL1) and other related derivatives, the probable enzyme residues engaged in interaction with the peptides were defined based on the crystal structure of the complex of cathepsin D with its inhibitor pepstatin [43] and an earlier study [44]. Interaction site residues corresponding to positions P2 and P3 of the PCLs (the scissile residues being P1-P1′; Table 1) were identified as: Ser 80, Gly 225, Thr 226, Phe 118, Val 230, Met 299, Met 301, Ile 312, Gln 14 and Ser 227. The method employs a coarse-grained representation to generate the initial models which are then refined using a Monte Carlo procedure. The best structural model for the enzyme – PCL1 complex was selected by comparison with the crystal structure of cathepsin D - pepstatin complex so that the corresponding residues of both the ligands had the best-fit match.

Molecular visualization and structural superposition were performed with the UCSF Chimera package [45]. Finally, the best structural models of the cathepsin D - PCL complexes were subjected to high-resolution refinement using the Rosetta FlexPepDock protocol [46,47] and the top models were utilized for analysis. PCL8 and its close derivative, PCL8-b were modelled with phenylalanine at P1′ position *in-lieu* of nitro-phenylalanine as the program was limited to account for only natural amino acid residues. Also, PCL1 was modeled *sans* the *C*-terminal Arg 11 as our assay results showed it to have little impact on enzymatic cleavage rate and to allow better structural comparison between peptides of similar sequence length. For consideration of interactions between cathepsin D and the peptides, slightly liberal cut-off distances were applied considering the macromolecular nature of structures and the fact that the structural complexes were obtained by computational methods. Non-conventional interactions were also considered in our analyses.

3. Results

3.1. Peptide cleavage in the RPE cell homogenate

A set of peptide substrates (Table 1) with putative sensitivity to cathepsin D were subjected to cleavage assay in the ARPE-19 homogenate. The aim was to utilize these substrates as 'peptide-based cleavable linkers' (PCL) for cargo attachment and controlled release in the RPE cells as there is cathepsin D activity in the RPE cells [35]. Although the PCLs were chosen to be sensitive to cathepsin D, they could as well possibly undergo cleavage by the concerted action of intracellular proteases. The peptides were labeled with a FRET pair (EDANS/Dabcyl) for monitoring the peptide cleavage using fluorescence (Scheme 3).

The PCL sequences showed varying rates of cleavage (Fig. 1). It is remarkable that some PCLs are cleaved almost completely in the RPE homogenate within 1–2 h (e.g. PCL 1, PCL 5), whereas others show moderate to slow cleavage rates (e.g. PCL 10, 40% in 48 h; PCL 8, less than 10% in 48 h).

3.2. PCL conjugates with cell penetrating peptides

Intracellular delivery depends on the ability to transport the drug across the plasma membrane. A set of four CPPs selected from literature precedence [48–50] were used to construct twelve chimeras (4 CPPs attached to 3 PCLs) by fusing CPPs to the *N*-terminus of the PCL peptides (Scheme 2). Based on PCL cleavage rates (Fig. 1), two rapid cleaving (PCL1, PCL5) and one slow cleaving (PCL10) sequences were chosen for conjugation with CPPs. The selected PCLs were not toxic to the ARPE-19 cells (Fig. 2) and were armed with the FRET pair (Dabcyl/EDANS) to facilitate easy read out of the cleavage assays with the CPP-PCL chimeras. The CPP-PCL chimeras were tested for their cleavage propensity in the ARPE-19 cell homogenate. PCL1 and PCL5 containing chimeras cleaved rapidly compared to the PCL 10 (Fig. 3).

No significant changes in the cleavage rates were seen for the CPP-PCL chimeras as compared to the native PCLs. Strikingly, though, a significant difference in the relative degree of cleavage of PCL1 and PCL5 was observed as compared to their conjugated form with CPP1. It is plausible that CPP1 influences the access of the PCL1 cleavage site by cathepsin D either sterically or by inducing a conformational change. In the case of CPP1-PCL5, there could be a modest increase in cleavage rate of PCL5 effected by CPP1 that could result in aggregation leading to enhanced 'fluorescence' [51,52].

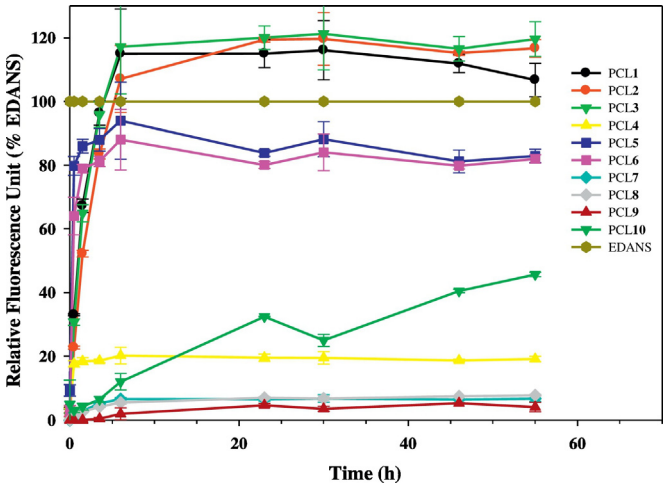

Fig. 1. Enzymatic assay of PCLs in ARPE-19 cell lysate. PCLs were incubated with cell lysate and fluorescence intensity from EDANS was recorded over time (*Ex*: 340 nm; *Em*: 490 nm). Data was normalized to that of free EDANS. Error bars represent mean ± standard deviations for $n = 3$.

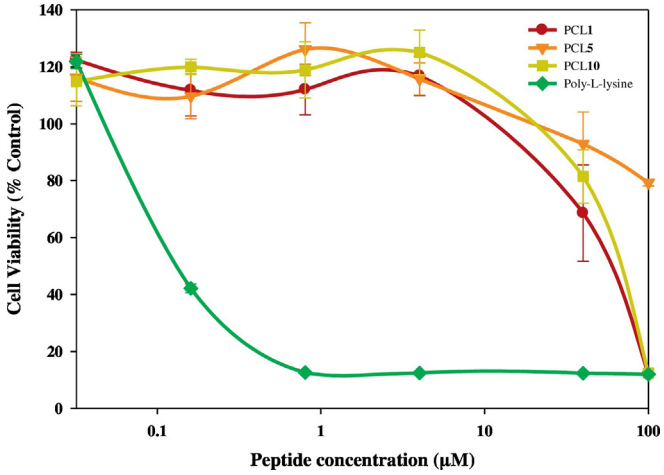

Fig. 2. Cytotoxicity of PCLs in ARPE-19 cells. Cells were treated with peptides for 5 h and cell viability was evaluated with MTT cytotoxicity assay. Data was normalized based on the viability of untreated cells. Data are represented as mean ± SD ($n = 3$).

3.3. Uptake of PCL and CPP-PCL peptides into the RPE cells

Fluorescence assisted cell sorting (FACS) analyses were carried out to determine cellular uptake and subsequent cleavage of the peptides within cultured ARPE-19 cells. EDANS fluorescence (450/20 band pass filter) allowed estimation of the cleaved PCL fragments. No EDANS fluorescence was expected from native peptide chimeras due to FRET effect. The analyses showed increased cellular fluorescence intensity in ARPE-19 cells for the CPP conjugated PCL chimeras (Fig. 4) as compared to constructs without the CPPs (Supplementary material, Fig. S2). Interestingly, however, native PCL1 (without any CPP attached) showed significant cellular uptake (Supplementary material, Fig. S2). This was an intriguing observation and we decided to include PCL1 in its native form in further cargo release studies. All CPP-PCL chimeras were non-toxic in the ARPE-19 cells (Supplementary material, Fig. S3, data shown only for the two chimeras used for further conjugation with cargoes).

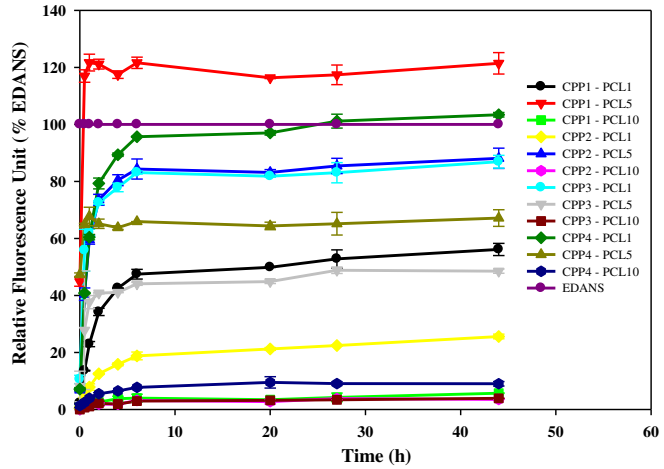

Fig. 3. Enzymatic cleavage of CPP-PCL chimeras in ARPE-19 cell lysate. The conjugates were incubated with cell lysate and EDANS fluorescence as a measure of PCL cleavage was detected at different time points (*Ex*: 340 nm; *Em*: 490 nm). Fluorescence of EDANS increased over time as a result of proteolytic cleavage of PCLs and consequent dequenching of EDANS. The fluorescence intensities were normalized based on the total fluorescence of free EDANS. Error bars represent mean ± standard deviations for $n = 3$.

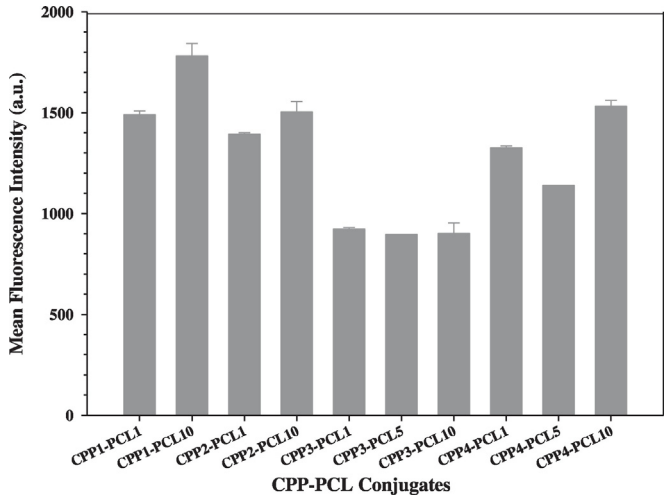

Fig. 4. Uptake of CPP-PCL chimeras (5 μM) by ARPE-19 cells. Following 1 h of incubation at 37 °C, cells were washed and mean fluorescence intensity of EDANS in the living cells was measured by flow cytometry. Mean values of three independent experiments, each performed in triplicate, are shown. Conjugates CPP1-PCL5 and CPP2-PCl 5 were found to have toxicity at concentration 5 μM and higher and were not included in the cellular uptake assay.

3.4. Stability of CPP-PCL chimeras in the vitreous

In vitro stability of the CPP-PCL chimeras was tested in ex vivo porcine vitreous. All the chimeras were stable in the porcine vitreous for more than 6 days (Supplementary material, Fig. S4). This is important because upon intravitreal injection, the PCLs should/need to be chemically stable in the vitreal environment and be able to release the cargo only after their cellular entry.

3.5. Cargo release from the peptide conjugates

For cargo release studies, two representative chimeric peptides were chosen: CPP1-PCL1 (fast cleaving) and CPP1-PCL10 (slow cleaving). The same CPP was used in both chimeras to enable comparisons of the intrinsic cleavage propensity of the PCLs and exclude the effects of the anchoring CPP sequence. PCL1 was also included in the release studies since it showed cellular uptake without an anchoring CPP. Two D-pentapeptide sequences were chosen as cargoes because they are enzymatically stable and afforded easy conjugation at the C-terminus of CPP-PCL chimeras. This strategy enabled quantitative LC-MS analyses of the intact D-peptide (cargoes) after their enzymatic release. Lipophilic (fwpVl: log D = +2.0) and hydrophilic (ynaVl: log D = −2.0) D-pentapeptide sequences were used as cargo prototypes in six conjugates (Table 2). The released fragments in the ARPE-19 cells were identified from whole cell lysates by LC-QTOF/MS analysis. For each cargo, two fragments were detected, containing one or two carry over residues from the PCL sequences. The hydrophobic cargo fwpVl was detected as fragments rfwpVl and KrfwpVl and the hydrophilic cargo ynaVl as fragments rynaVl and KrynaVl. The detected fragments and their corresponding masses are listed in Table 2.

The released cargo fragments were quantitated in whole cell lysate after 1 h exposure of the ARPE-19 cells with cargo conjugates. CC-3 and CC-4 showed greater cargo release than CC-5 and CC-6 for both hydrophilic and hydrophobic cargoes (Fig. 5A, B). CC-3 and CC-4 contain PCL1, the fast cleaving linker, whereas CC-5 and CC-6 include the slow cleaving PCL10. Different levels of cargo release from these conjugates could be attributed to the PCL sequence.

Released levels of cargo D-peptides from CC-1 and CC-2 were low (Fig. 5A, B). CC-1 and CC-2 contain only native PCL1 without CPP. This was an unexpected result because PCL1 showed high cellular uptake and rapid cleavage in the cell homogenate (Fig. 1 & Supplementary material, Fig. S2) using FACS based technique. We postulate that unlike CPP chimeras, CC1 and CC2 may not be accessible to the enzymes in the intact cells.

In the second experiment, intact RPE monolayer was mimicked. ARPE-19 cells were cultured on laminin coated filters to a polarized tight epithelium. The cargo conjugates (CC1–CC6) were placed to the apical side of the monolayer and sampled from the basolateral compartment at different time points (Fig. 6A). The results followed the same trend as seen in the whole cell lysates. Higher amounts of released cargo fragments were recorded from the basolateral side after CC-3 and CC-4 administration than from CC-5 and CC-6 (Fig. 6B, C). The cargo fragments gradually accumulated to the basolateral side of the RPE blood-retinal model. No significant release of cargo fragments was seen after administration of CC-1 and CC-2 (Fig. 6B, C). These observations validate that the fast cleaving PCL1 results in faster cellular cargo release than the slowly cleaving PCL10 in the case of CPP-PCL conjugates. Apparently, PCL1 without cell penetrating peptide does not reach the cleaving enzymes in the RPE monolayer.

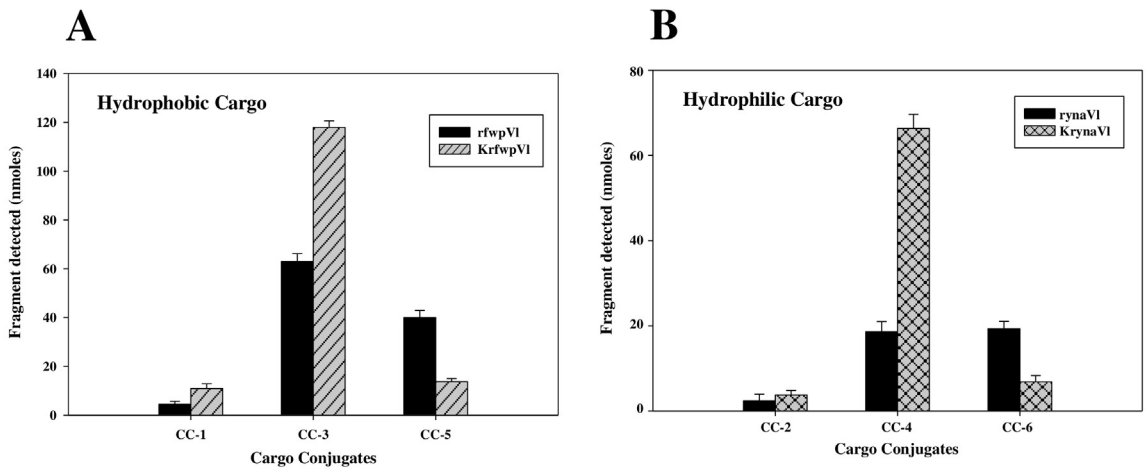

Fig. 5. Quantitative estimation of (A) hydrophobic and (B) hydrophilic cargo release in ARPE-19 cell lysates. Intracellular concentrations of cargo fragments were determined after ARPE-19 cells were incubated with cargo conjugates (5 μM) at 37 °C for 1 h. Following cell lysis, the intracellular concentrations of cargo fragments released were estimated with LC–MS. Fragment concentrations were calculated from the peak area ratio of non-labeled to labeled fragments (internal standard). The results are average values of two repeats with three parallel samples each. The error bars represent standard deviations between repeats.

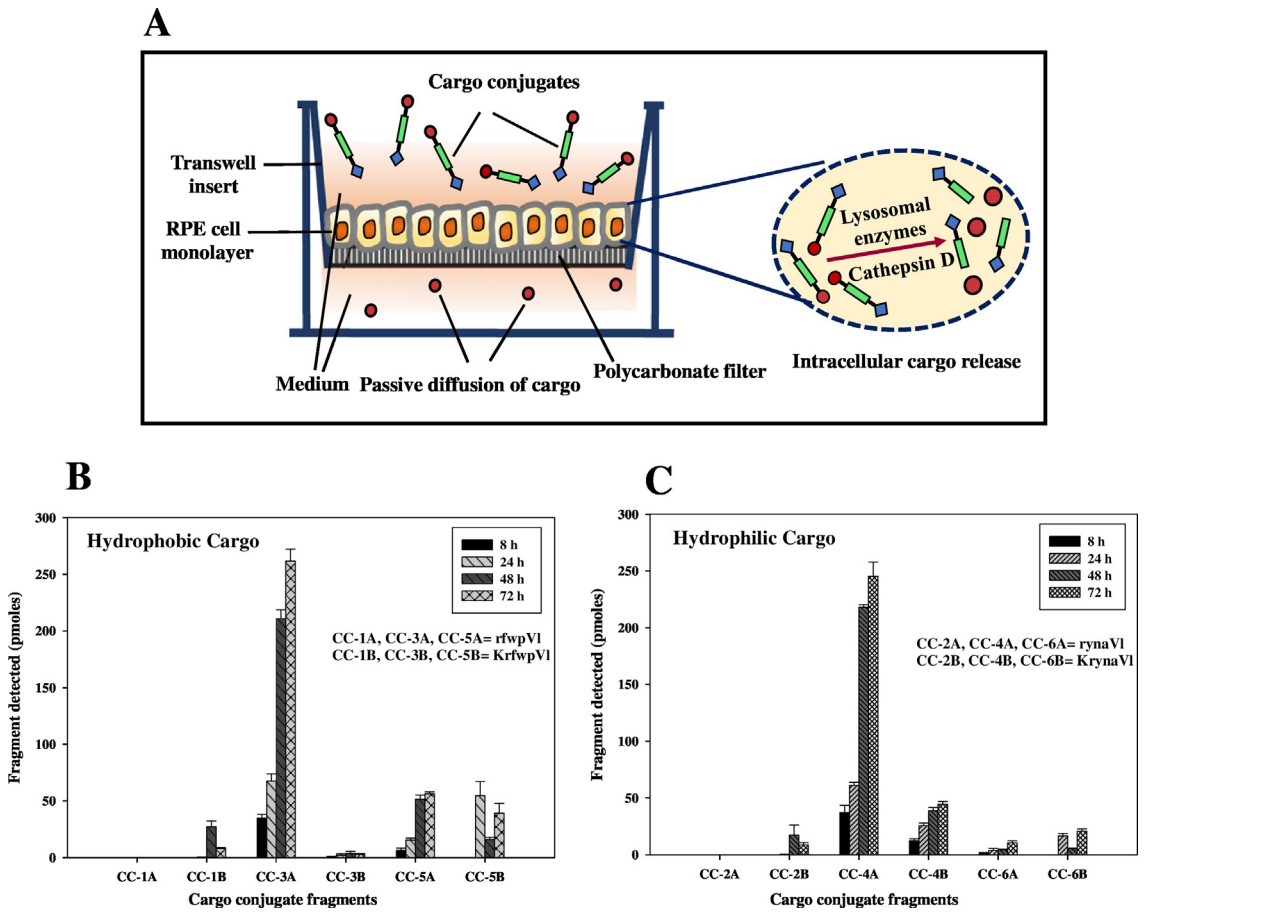

Fig. 6. (A) Quantitative estimation of cargo fragments from the basolateral chamber in filter cultured ARPE-19 cells (blood-retina-barrier model). Filter cultured ARPE-19 cells were incubated with cargo conjugates (5 μM) at 37 °C for 1 h. Concentrations of cargo fragments (B) hydrophobic and (C) hydrophilic were determined at different time points by LC–MS. Fragment concentrations were calculated from the peak area ratio of non-labeled to labeled fragments (internal standard). The results are average values of two repeats with three parallel samples each. The error bars represent standard deviations between repeats.

The results also point out that both hydrophobic and hydrophilic cargoes can be transported and released in the intracellular environment of ARPE-19 cells using PCL linkers. Higher amounts of hydrophobic cargoes were seen than the hydrophilic cargo peptide fragments in the basolateral compartment after administration of similar conjugate system (i.e. CC-3 vs CC-4 and CC-5 vs CC-6) (Fig. 6B, C). It seems that the hydrophobic cargo is released faster than the hydrophilic cargo within the cells, the released hydrophobic cargo probably also permeates faster across the plasma membrane to the basolateral compartment.

3.6. Structure-activity relationship of PCLs

To understand the structural requirements of PCLs for cathepsin D mediated cleavage, analogs of the parent PCLs with natural and unnatural amino acid residues were studied using enzymatic assays and computational modeling. Previous studies indicated the preference for certain amino acids at or near the scissile bond (P1, P1′, P2, P2′ and P3, P3′ and P5, P5′) positions [44,53,54]. Thus, several analogs of fast cleaving (PCL1) and slow cleaving (PCL8, PCL10) with natural and unnatural amino acid substitutions were subjected to cathepsin D mediated enzymatic cleavage assay in ARPE-19 homogenate (Table 3).

The effects of amino acid substitutions are expressed as relative increase or decrease in the enzymatic cleavage value of the PCL analogs at a certain time point (4 h) as compared to the parent PCL. The results are depicted as relative fluorescence unit (% EDANS) in Fig. 7. Notably, analogs PCL1-b and PCL1-c showed a significant reduction in cleavage rates as compared to the parent PCL1. The analogs of the moderately cleaving PCL10 namely, PCL10-a and PCL10-d retained their enzymatic activity; in fact, they showed a modest increase. The results suggest that the substitutions at P1-P1′ sites in PCL10-a and at the P2 site in PCL10-d are well tolerated with slightly increased enzymatic activity.

The computational model supports the notion that increased hydrophobicity at the P2 site might increase the peptide's sensitivity to cleavage. Residues Met 299, Met 301, Val 230, Leu 228, Ile 312 and Thr 226 present a hydrophobic pocket for interaction with the side chains of the residue at P2. In the case of PCL1, hydrophobic interaction of the

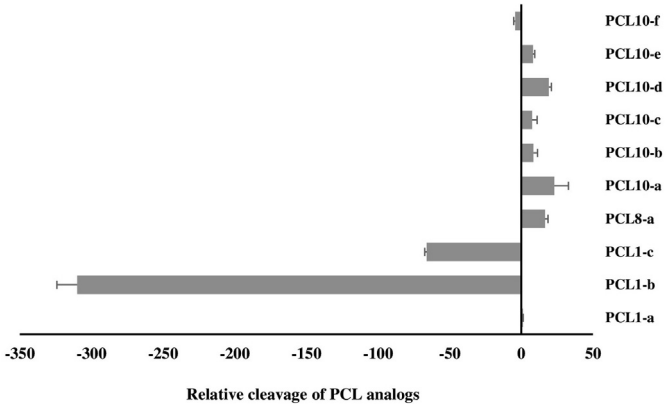

Fig. 7. Enzymatic cleavage assay of PCL analogs. Increase or decrease (fold) in the enzymatic cleavage value relative to the parent peptide at 4 h is shown. Each assay was performed in triplicate and the average values have been presented.

Leu5 side-chain with the side-chains of cathepsin D residues namely, Met 299 and Met 301 is significant. In addition, the backbone of Leu 5 is stabilized by a weak C—H···O hydrogen bond from the donor Ser 80. Interestingly, the P1 site residue, Phe 6 makes contact with the catalytic residues Asp 33 and Asp 223 via two weak non-covalent interactions; lone-pair(anion)···π and the C—H···O hydrogen bond. Phe 6 is stabilized by a network of weak non-conventional interactions and a conventional H-bond (Table 4). Both the P1′ and P2′ residues of PCL-1, namely Phe 7 and Arg 8 mediate contacts with cathepsin D through a combination of hydrophobic forces, weak non-covalent interactions and strong H-bond. In particular, Phe 7 is an acceptor of two C—H···π contacts with the enzyme residue Ile303 and the side chain of Arg 8 is stabilized by two strong N—H···O hydrogen bonds. Overall, a plethora of weak interactions, hydrophobic forces and a few strong hydrogen bonds form the basis of peptide recognition and catalysis (Fig. 8, Table 4).

4. Discussion

Current therapeutic approaches to deliver drugs to the retina and choroid utilize local intravitreal injections. Frequent injections are not desirable for reasons of patient compliance and burden to the healthcare. Thus, a significant challenge is to maintain therapeutic levels of the drugs for prolonged periods [29,55]. Duration of drug action can be increased with controlled release formulations (e.g. intraocular implants), but these technologies do not augment delivery of poorly permeating drugs to the intracellular space. Often development projects are discontinued due to the inadequate tolerance of the carrier materials in the eye. New safer delivery systems for prolonged and intracellular drug delivery are needed in the field of retinal and choroidal drug treatment.

The RPE is a key therapeutic target cell in several diseases, e.g. viral infections, dry AMD, proliferative vitreoretinopathy and some retinal degenerations [56–58]. Also, the choroid is an important drug target, for example in the neovascular conditions (e.g. the wet form of AMD). For these reasons, we envisioned a strategy for intracellular drug release within the RPE cells with enzymatically cleaving peptide linkers. The released drug could target intracellular components or alternatively the RPE cells might form a depot of the released cargo that diffuses to the surrounding tissues (e.g. neural retina, choroid) (Fig. 6). The rate of cargo release from the RPE cells can be controlled by modulating the cleavage of PCLs. The strategy draws a parallel with the approach of transfecting the corneal epithelium and the RPE for continued expression and secretion of bioactive agents [59,60] but with the advantage that exogenous molecules could be released with control based on PCL sequence.

Table 4
Non-covalent interactions between PCL1 and cathepsin D residues in the structural model of the complex. Interactions involving residues in positions P2-P1-P1′-P2′ are listed.

Site	Substrate residue	Cathepsin D residue	Distance (Å)/Angle (°)	Interaction type
P1	Phe 6/HD1	Thr 226/N	2.7/145.3	C—H···N
	Phe 6/HD1	Thr 226/OG1	3.3/130.1	C—H···O
	Phe 6/HE1	Gly 225/O	2.7/121.8	C—H···O
	Phe 6/centroid	Asp 33/OD2	3.7	lp(anion) ···π
	Phe 6/1HB	Asp 223/OD2	3.0/145	C—H···O
	Phe 6/1HB	Thr 226/OG1	2.8/127.5	C—H···O
	Phe 6/H	Thr 226/OG1	2.0/150.8	N—H···O
	Phe 6/O	Ile 312/3HD1	2.8/144.1	O···H—C
	Phe & HA	Tyr 78/O	3.0/144.1	C—H···O
P2	Leu 5/CD1	Met 301/SD	3.5	Hydrophobic
	Leu 5/CD1	Met 299/SD	4.6	Hydrophobic
	Leu 5/O	Ser 80/2HB	2.3, 157.6	O···H—C
	Leu 5/CD2	Thr 226/CG2	3.6	Hydrophobic
	Leu 5/CD2	Leu 228/N	3.5	Van der Waals
	Leu 5/3HD1	Met 301/SD	2.9/130.4	C—H···S
P1′	Phe 7/H	Tyr 78/O	2.0/122.7	N—H···O
	Phe 7/O	Tyr 78/HA	3.3/115.6	O···H—C
	Phe 7/2HB	Tyr 78/O	2.7/123.3	C—H···O
	Phe 7/centroid	Ile 303/3HG2	3.2	C—H···π
	Phe 7/centroid	Ile 303/2HD1	3.1	C—H···π
	Phe 7/HE1	Ser 307/OG	2.3/144.1	C—H···O
P2′	Arg 8/1HB	Ser 36/N	3.2/141.1	C—H···N
	Arg 8/1HB	Ser 36/OG	3.3/147.9	C—H···O
	Arg 8/1HG	Ile 134/O	3.3/123.8	C—H···O
	Arg 8/HE	Ser 36/OG	2.0/149.1	N—H···O
	Arg 8/2HH1	Val 136/N	2.7/148.9	N—H···N
	Arg 8/1HH2	Ser 36/OG	1.9/140.9	N—H···O

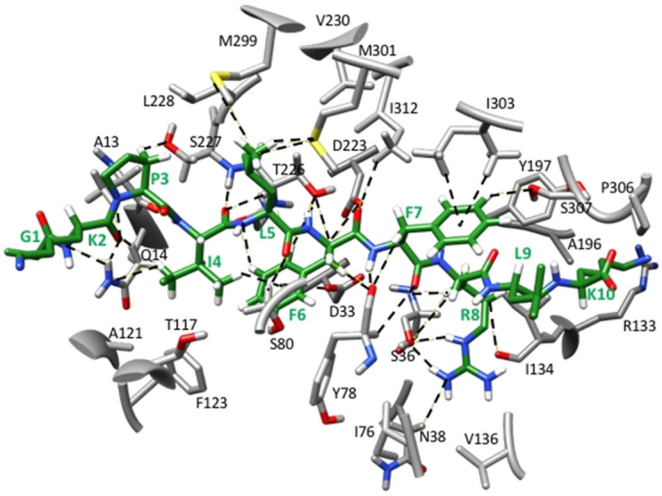

Fig. 8. Non-covalent interactions of PCL1 (green) at the cathepsin D (grey) catalytic site. PCL1 residues are labeled in green. (For interpretation of the references to colour in this figure legend, the reader is referred to the web version of this article.)

For the purpose of intracellular cargo release by enzymatic cleavage, PCL sequences with varying sensitivity to cathepsin D were selected. Cathepsin D, a lysosomal enzyme, has high expression levels in RPE cells but not present in the vitreous [35]. Increased activity of cathepsin D with aging has been reported [61]. Intracellular uptake was facilitated by conjugating CPPs with PCLs harboring cargo. D-pentapeptide cargoes were chosen for ease of synthesis, resistance to proteolytic cleavage to facilitate detection and easy manipulation of sequence to effect changes in physicochemical properties of the cargo prototypes (hydrophobic/hydrophilic). Our studies identified PCLs and CPP-PCL chimeras that showed intracellular localization and differential rates of cargo release in the ARPE-19 cells. The chimeras were non-toxic to the ARPE-19 cells and stable in porcine vitreous ex vivo. The fast cleaving CPP-PCL chimeras released the cargo inside the ARPE-19 cells for at least three days as the cleavage seems to continue during the time period 0–72 h. It is likely that the slow cleaving CPP-PCL chimeras release the cargo much longer than 72 h because the cleavage rate was slow. Although it is difficult to predict the total duration of complete release, depending on the initial dosing the strategy seems to have the potential to release the cargo for at least weeks. Obviously, slow release rates are desirable for highly potent compounds that are capable of exerting their actions at low concentrations. A fast release would be preferable for compounds that act by turning on some biochemical mechanism that will then prevail for a long time. Our estimates show that for 'nanomoles' of the cargo within the RPE cells, 'picomoles' of passively diffusing cargo from the RPE (to the basolateral compartment) is detected over a time period of 72 h. Considering moderate recovery loss due to technical limitations, this still holds promise for sustained release over a long period of time.

Earlier studies on intracellular cargo delivery relied on fluorescence microscopy or flow cytometry to establish cargo delivery [62–66]. Other studies too have used secondary read out effects such as anti-proliferative effects of cancer drugs [67] or changes in the protein expression after siRNA delivery [68] as validation of cargo delivery. In our present study, we demonstrate accurate quantification of intracellular cargo release using LC-MS, like we did previously for liposomes in the cancer cells [69]. To the best of our knowledge, this is the first report

that directly quantitates cargo release from conjugated peptide linkers in the intracellular and extracellular space. We postulate that the methodology has general applicability to other cell types and therapeutic agents.

To understand the structural requirements of the PCLs we carried out computational modeling. The enzyme-PCL complexes revealed the significance of weak non-covalent interactions at the catalytic site. This is in tune with the growing realization of the importance of such forces in biomolecular recognition and activity [70–73]. It was intriguing to find a rationale for the lack of enzymatic cleavage of PCL8 (GSPIVF*NphRL). This was particularly so in light of the fact that a closely related peptide, PCL8-b (KPIVF*NphRL), in an earlier study showed moderate levels of substrate activity [44]. We compared the structural models of PCL1, PCL8 and the related PCL8-b in complex with cathepsin D (Fig. 9). All three peptides seem to be able to present their epitopes for enzymatic cleavage and the striking differences arise from the positioning of the long side-chain of the *N*-terminus Lys 2/Lys 1 (PCL1/PCL8-b). In the PCL-1 complex, Lys 2 backbone is stabilized by cathepsin D by virtue of a strong donor H-bond (N—H···O) from Gln 14 and a few weak donor H-bonds (N—H···N & C—H···O) from Gln 14 and Ala 13. Even though the long side chain of Lys 2 does not contact the enzyme residues, several possible rotamers are feasible that enhances the accessible conformational space of the Lys 2 side chain. The lysine side chain is thus capable of forming both hydrophobic, weak non-covalent interactions and hydrogen bonds with neighboring enzyme residues. A similar possibility exists for the *N*-terminus Lys 1 in the PCL8-b complex. However, in PCL8, the short side chain of serine has only a few rotamers and consequently a limited accessible conformational space. These factors reduce the chance of stabilizing contacts of the Ser 2 with neighboring enzyme residues. Apparently, the long side chain of the Lys 2 residue anchors the peptides (PCL1, PCL8-b) within the catalytic site of cathepsin D facilitating the register of the cleavable epitopes for catalysis.

The structural models also provide a rationale for the 70-fold loss of catalytic activity in PCL1-c, wherein the P1 and P1′ residues are substituted with tryptophan. A comparison of the top models for both the complexes, PCL1 and PCL1-c with cathepsin D (Fig. 10A, B) seem to suggest that the introduction of Trp-Trp results in conformational mobility of the peptide. This necessitates a conformational rearrangement of the enzyme with the possibility of disturbing the delicate interactions at the active site. A similar rationale might hold true for the 300-fold loss of activity in the napthylalanine substituted peptide (PCL1-b).

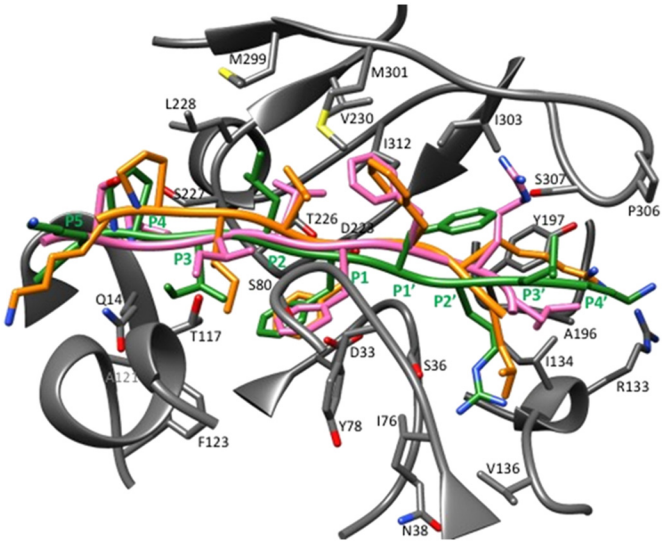

Fig. 9. Superposition of structural models of PCL1 (green), PCL8 (pink) and PCL8-b (orange) at the catalytic site of cathepsin D (grey). Peptide sites are labeled in green colour. (For interpretation of the references to colour in this figure legend, the reader is referred to the web version of this article.)

The residence time of injected drugs in the vitreous depends on the molecular size [74]. Retention of peptides is less than six days indicating that the peptide chimeras would not release the cargo prematurely within the vitreous humor. Cargo release is expected to take place within the RPE cells where we determined the release kinetics for 72 h. Fast cleaving PCLs released cargo much faster than the slow cleaving PCLs indicating that it would take longer to release whole cargo from the slow cleaving PCLs. The release will last for much longer than 72 h because the quantity of the released peptides within the RPE cells was estimated to be nanomoles (Fig. 5) whereas picomole amounts were detected in the extracellular space (Fig. 6). In the case of specific drugs, these dosing considerations are complicated and affected by many factors. For subconjunctival administration 1–2 weeks' dosing intervals is fine, while one month or longer is preferable for intravitreal administration. Different drugs have specific effective concentrations and local clearance rates that determine the required rate of delivery. Finally, some drugs require constant drug exposure, but some molecules turn on the biochemical event and result in activity of weeks after local drug delivery [75]. We have shown here a new concept for intracellular drug release in the RPE. Future studies will shed light on how this concept could be utilized for specific drugs and treatments.

Ocular drug delivery systems often exhibit desirable release properties, but still lack translational success. Among other aspects, one major cause that limits their application in vivo is toxicity arising from synthetic polymeric materials, their degradation products or carry-over additives from drug formulation. In other instances, physicochemical properties of the drug molecules were exploited to form depots for sustained release, but this is applicable only in specific cases [76,77]. We report here a peptide-based delivery system that utilizes the cellular environment of the RPE cells to act as a reservoir for controlled release of cargo fragments to the extracellular/choroidal space. The peptide based delivery system is non-toxic, stable in porcine vitreous and does not rely on the physicochemical properties of a particular drug molecule for binding to cellular components. The efficacy of cargo delivery would depend upon the mechanism of cellular uptake and consequently lysosomal trafficking. Differentially cleaving linkers offer the advantage of modulating the rate of cargo release intracellularly thereby facilitating drug delivery to the intracellular targets. To the best of our knowledge, this is the first report to demonstrate the utility of RPE cells to act as a reservoir for controlled release of exogenous drugs. Small molecule drugs are rapidly cleared within the vitreous and the strategy to utilize the RPE cells for controlled release would increase the duration of drug activity. Although small molecules and peptides are likely to diffuse out from the RPE cells (depot action that we have highlighted), delivery of therapeutic proteins for targeting intracellular components too can be an exciting prospect [36].

5. Conclusions

We highlighted a peptide-based strategy for sustained drug release utilizing the intracellular space as a depot in the ocular context. While in most cases drug release from intracellular depots, such as nanoparticles, is spontaneous and poorly controlled, our approach of using differentially cleaving peptide sequences as linkers to the cargo drug allows pre-designed control of the release rates. Also, the strategy does not depend on the physicochemical properties of a particular drug and thus presents a broad applicability as long as the drug can be linked to the peptides. Specific cell type targeting moieties or grafting of the PCLs onto biodegradable polymers may further future applications of this technology.

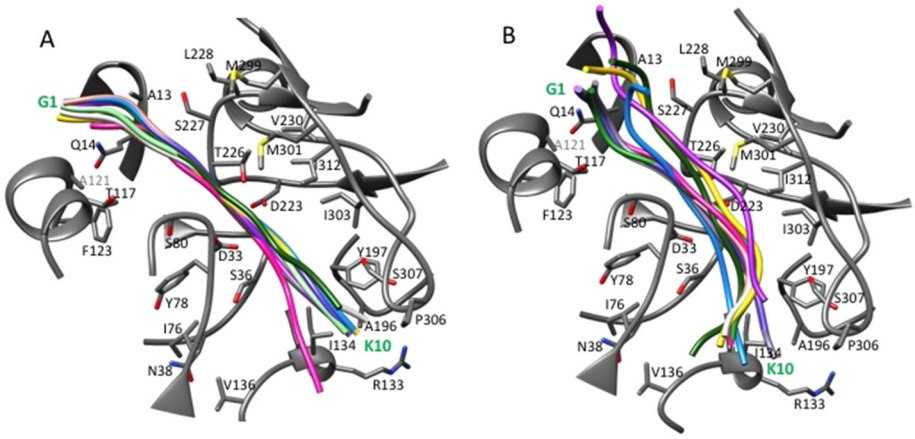

Fig. 10. Superposition of top ten structural models (A) PCL1 and (B) PCL1-c at the catalytic site of cathepsin D (grey).

Supplementary data to this article can be found online at http://dx.doi.org/10.1016/j.jconrel.2017.02.013.

Conflict of interest statement

The authors declare no conflict of interest.

Acknowledgements

We thank Leena Pietilä for technical support and Tiina Pessa-Morikawa for assistance in performing the cell uptake studies. We are also grateful to Miia Reponen for LC-MS measurements. This work was funded and supported by Academy of Finland (Grant no. 263573) (ModDrug consortium).

References

[1] D.M. Maurice, S. Mishima, Ocular pharmacology, in: M. Sears (Ed.), Handb. Exp. Pharmacology, Springer-Verlag, Berlin-Heidelberg 1984, pp. 16–119.
[2] A.V. Chappelow, P.K. Kaiser, et al., Drugs 68 (2008) 1029–1036.
[3] V. Sarao, D. Veritti, F. Boscia, P. Lanzetta, V. Sarao, D. Veritti, F. Boscia, P. Lanzetta, Intravitreal steroids for the treatment of retinal diseases, Sci. World J. 2014 (2014) 989501.
[4] G.M. Keating, Aflibercept: a review of its use in diabetic macular oedema, Drugs 75 (2015) 1153–1160.
[5] J.E. Frampton, Aflibercept for intravitreal injection, Drugs Aging 29 (2012) 839–846.
[6] V.-P. Ranta, A. Urtti, Transscleral drug delivery to the posterior eye: prospects of pharmacokinetic modeling, Adv. Drug Deliv. Rev. 58 (2006) 1164–1181.
[7] S. Einmahl, M. Savoldelli, F. D'Hermies, C. Tabatabay, R. Gurny, F. Behar-Cohen, Evaluation of a novel biomaterial in the suprachoroidal space of the rabbit eye, Invest. Ophthalmol. Vis. Sci. 43 (2002) 1533–1539.
[8] T.W. Olsen, X. Feng, K. Wabner, S.R. Conston, D.H. Sierra, D.V. Folden, M.E. Smith, J.D. Cameron, Cannulation of the suprachoroidal space: a novel drug delivery methodology to the posterior segment, Am. J. Ophthalmol. 142 (2006) 777–787 (e2).
[9] N. Kuno, S. Fujii, Recent advances in ocular drug delivery systems, Polymers (Basel) 3 (2011) 193–221.
[10] R. Gaudana, H.K. Ananthula, A. Parenky, A.K. Mitra, Ocular drug delivery, AAPS J. 12 (2010) 348–360.
[11] H.F. Edelhauser, C.L. Rowe-Rendleman, M.R. Robinson, D.G. Dawson, G.J. Chader, H.E. Grossniklaus, K.D. Rittenhouse, C.G. Wilson, D.A. Weber, B.D. Kuppermann, K.G. Csaky, T.W. Olsen, U.B. Kompella, V.M. Holers, G.S. Hageman, B.C. Gilger, P.A. Campochiaro, S.M. Whitcup, W.T. Wong, Ophthalmic drug delivery systems for the treatment of retinal diseases: basic research to clinical applications, Investig. Opthalmol. Vis. Sci. 51 (2010) 5403.
[12] U.B. Kompella, A.C. Amrite, R. Pacha Ravi, S.A. Durazo, Nanomedicines for back of the eye drug delivery, gene delivery, and imaging, Prog. Retin. Eye Res. 36 (2013) 172–198.
[13] E. Eljarrat-Binstock, J. Pe'er, A.J. Domb, New techniques for drug delivery to the posterior eye segment, Pharm. Res. 27 (2010) 530–543.
[14] I. Surgucheva, N. Ninkina, V.L. Buchman, K. Grasing, A. Surguchov, Protein aggregation in retinal cells and approaches to cell protection, Cell. Mol. Neurobiol. 25 (2005) 1051–1066.
[15] K. Kaarniranta, J. Hyttinen, T. Ryhanen, J. Viiri, T. Paimela, E. Toropainen, I. Sorri, A. Salminen, Mechanisms of protein aggregation in the retinal pigment epithelial cells, Front. Biosci. 2 (2010) 1374–1384.
[16] A. Kauppinen, From protein aggregation to inflammasome activation in RPE cells, Acta Ophthalmol. 92 (2014).
[17] L. Sun, Peptide-based drug development, Mod. Chem. Appl. 1 (2013).
[18] D. Reischl, A. Zimmer, Drug delivery of siRNA therapeutics: potentials and limits of nanosystems, Nanomedicine 5 (2009) 8–20.
[19] H.-Y. Zhou, J.-L. Hao, S. Wang, Y. Zheng, W.-S. Zhang, Nanoparticles in the ocular drug delivery, Int. J. Ophthalmol. 6 (2013) 390–396.
[20] N.Ü. Okur, E.H. Gökçe, Lipid nanoparticles for ocular drug delivery, Int. J. Ophthalmic Res. 1 (2015) 77–82.
[21] A. Patel, M. Patel, X. Yang, A.K. Mitra, Recent advances in protein and peptide drug delivery: a special emphasis on polymeric nanoparticles, Protein Pept. Lett. 21 (2014) 1102–1120.
[22] S. Loukovaara, P. Koivunen, M. Inglés, J. Escobar, M. Vento, S. Andersson, Elevated protein carbonyl and HIF-1α levels in eyes with proliferative diabetic retinopathy, Acta Ophthalmol. 92 (2014) 323–327.
[23] L. Pitkänen, J. Pelkonen, M. Ruponen, S. Rönkkö, A. Urtti, Neural retina limits the nonviral gene transfer to retinal pigment epithelium in an in vitro bovine eye model, AAPS J. 6 (2004) 72–80.
[24] L. Pitkänen, M. Ruponen, J. Nieminen, A. Urtti, Vitreous is a barrier in nonviral gene transfer by cationic lipids and polymers, Pharm. Res. 20 (2003) 576–583.
[25] Q. Xu, N.J. Boylan, J.S. Suk, Y.-Y. Wang, E.A. Nance, J.-C. Yang, P.J. McDonnell, R.A. Cone, E.J. Duh, J. Hanes, Nanoparticle diffusion in, and microrheology of, the bovine vitreous ex vivo, J. Control. Release 167 (2013) 76–84.
[26] P. Mitchell, J.-F. Korobelnik, P. Lanzetta, F.G. Holz, C. Prünte, U. Schmidt-Erfurth, Y. Tano, S. Wolf, Ranibizumab (Lucentis) in neovascular age-related macular degeneration: evidence from clinical trials, Br. J. Ophthalmol. 94 (2010) 2–13.
[27] R. Sophie, A. Akhtar, Y.J. Sepah, M. Ibrahim, M. Bittencourt, D.V. Do, Q.D. Nguyen, Aflibercept: a potent vascular endothelial growth factor antagonist for neovascular age-related macular degeneration and other retinal vascular diseases, Biol. Ther. 2 (2012) 3.
[28] E.W.M. Ng, D.T. Shima, P. Calias, E.T. Cunningham, D.R. Guyer, A.P. Adamis, Pegaptanib, a targeted anti-VEGF aptamer for ocular vascular disease, Nat. Rev. Drug Discov. 5 (2006) 123–132.
[29] E.M. del Amo, K.-S. Vellonen, H. Kidron, A. Urtti, Intravitreal clearance and volume of distribution of compounds in rabbits: in silico prediction and pharmacokinetic simulations for drug development, Eur. J. Pharm. Biopharm. 95 (2015) 215–226.
[30] V. Delplace, S. Payne, M. Shoichet, Delivery strategies for treatment of age-related ocular diseases: from a biological understanding to biomaterial solutions, J. Control. Release 219 (2015) 652–668.
[31] G.R. da Silva, S.L. Fialho, R.C. Siqueira, R. Jorge, A.S. da Cunha Júnior, Implants as drug delivery devices for the treatment of eye diseases, Braz. J. Pharm. Sci. 46 (2010) 585–595.
[32] T. Yasukawa, Y. Ogura, H. Kimura, E. Sakurai, Y. Tabata, Drug delivery from ocular implants, Expert Opin. Drug Deliv. 3 (2006) 261–273.
[33] T. Yadav, T. Yadav, Microspheres as an ocular drug delivery system-a review, J. Drug Deliv. Ther. 3 (2013).
[34] A. Patel, Ocular drug delivery systems: An overview, World J. Pharmacol. 2 (2013) 47.
[35] P.E. Rakoczy, C.M. Lai, M. Baines, S. Di Grandi, J.H. Fitton, I.J. Constable, Modulation of cathepsin D activity in retinal pigment epithelial cells, Biochem. J. 324 (1997) 935–940.
[36] A. Dinca, W.-M. Chien, M.T. Chin, Intracellular delivery of proteins with cell-penetrating peptides for therapeutic uses in human disease, Int. J. Mol. Sci. 17 (2016) 263, http://dx.doi.org/10.3390/ijms17020263.
[37] V. Torchilin, Intracellular delivery of protein and peptide therapeutics, Drug Discov. Today Technol. 5 (2008) e95–e103, http://dx.doi.org/10.1016/j.ddtec.2009.01.002.
[38] E. Atherton, R.C. Sheppard, Solid Phase Peptide Synthesis: A Practical Approach, IRL Press at Oxford University Press, 1989.
[39] C. Guy, Optical Imaging Techniques in Cell Biology, second ed., 2012.

[40] E. Mannermaa, M. Reinisalo, V.-P. Ranta, K.-S. Vellonen, H. Kokki, A. Saarikko, K. Kaarniranta, A. Urtti, Filter-cultured ARPE-19 cells as outer blood–retinal barrier model, Eur. J. Pharm. Sci. 40 (2010) 289–296.
[41] M.B. Hansen, S.E. Nielsen, K. Berg, Re-examination and further development of a precise and rapid dye method for measuring cell growth/cell kill, J. Immunol. Methods 119 (1989) 203–210.
[42] A. Lamiable, P. Thévenet, J. Rey, M. Vavrusa, P. Derreumaux, P. Tufféry, PEP-FOLD3: faster de novo structure prediction for linear peptides in solution and in complex, Nucleic Acids Res. 44 (2016) W449–W454.
[43] E.T. Baldwin, T.N. Bhat, S. Gulnik, M.V. Hosur, R.C. Sowder, R.E. Cachau, J. Collins, A.M. Silva, J.W. Erickson, J.W. Erickson, Crystal structures of native and inhibited forms of human cathepsin D: implications for lysosomal targeting and drug design, Proc. Natl. Acad. Sci. U. S. A. 90 (1993) 6796–6800.
[44] P.E. Scarborough, K. Guruprasad, C. Topham, G.R. Richo, G.E. Conner, T.L. Blundell, B.M. Dunn, Exploration of subsite binding specificity of human cathepsin D through kinetics and rule-based molecular modeling, Protein Sci. 2 (1993) 264–276.
[45] E.F. Pettersen, T.D. Goddard, C.C. Huang, G.S. Couch, D.M. Greenblatt, E.C. Meng, T.E. Ferrin, UCSF Chimera—a visualization system for exploratory research and analysis, J. Comput. Chem. 25 (2004) 1605–1612.
[46] N. London, B. Raveh, E. Cohen, G. Fathi, O. Schueler-Furman, Rosetta FlexPepDock web server—high resolution modeling of peptide-protein interactions, Nucleic Acids Res. 39 (2011) W249–W253.
[47] B. Raveh, N. London, O. Schueler-Furman, Sub-angstrom modeling of complexes between flexible peptides and globular proteins, Proteins 78 (2010) 2029–2040.
[48] P.A. Wender, D.J. Mitchell, K. Pattabiraman, E.T. Pelkey, L. Steinman, J.B. Rothbard, The design, synthesis, and evaluation of molecules that enable or enhance cellular uptake: peptoid molecular transporters, Proc. Natl. Acad. Sci. U. S. A. 97 (2000) 13003–13008.
[49] X. Yang, S.K. Sarvestani, S. Moeinzadeh, X. He, E. Jabbari, Effect of CD44 binding peptide conjugated to an engineered inert matrix on maintenance of breast cancer stem cells and tumorsphere formation, PLoS One 8 (2013) e59147.
[50] H.-Y. Park, K.-J. Lee, S.-J. Lee, M.-Y. Yoon, Screening of peptides bound to breast cancer stem cell specific surface marker CD44 by phage display, Mol. Biotechnol. 51 (2012) 212–220.
[51] D. Wang, J. Qian, S. He, J.S. Park, K.-S. Lee, S. Han, Y. Mu, Aggregation-enhanced fluorescence in PEGylated phospholipid nanomicelles for in vivo imaging, Biomaterials 32 (2011) 5880–5888, http://dx.doi.org/10.1016/j.biomaterials.2011.04.080.
[52] A. Jadhav, R.S. Ferreira, C. Klumpp, B.T. Mott, C.P. Austin, J. Inglese, C.J. Thomas, D.J. Maloney, B.K. Shoichet, A. Simeonov, Quantitative analyses of aggregation, autofluorescence, and reactivity artifacts in a screen for inhibitors of a thiol protease, J. Med. Chem. 53 (2010) 37–51, http://dx.doi.org/10.1021/jm901070c.
[53] J.M. van Noort, A.C. van der Drift, The selectivity of cathepsin D suggests an involvement of the enzyme in the generation of T-cell epitopes, J. Biol. Chem. 264 (1989) 14159–14164.
[54] H. Sun, X. Lou, Q. Shan, J. Zhang, X. Zhu, J. Zhang, Y. Wang, Y. Xie, N. Xu, S. Liu, Proteolytic characteristics of cathepsin D related to the recognition and cleavage of its target proteins, PLoS One 8 (2013) e65733.
[55] E. Delamo, A. Urtti, Current and future ophthalmic drug delivery systems. A shift to the posterior segment, Drug Discov. Today 13 (2008) 135–143.
[56] C. Larcher, H. Recheis, R. Sgonc, W. Göttinger, H.P. Huemer, E.U. Irschick, Influence of viral infection on expression of cell surface antigens in human retinal pigment epithelial cells, Graefes Arch. Clin. Exp. Ophthalmol. 235 (1997) 709–716.
[57] A.C. Bird, Therapeutic targets in age-related macular disease, J. Clin. Invest. 120 (2010) 3033–3041.
[58] I. Bhutto, G. Lutty, Understanding age-related macular degeneration (AMD): relationships between the photoreceptor/retinal pigment epithelium/Bruch's membrane/choriocapillaris complex, Mol. Asp. Med. 33 (2012) 295–317.
[59] E. Toropainen, M. Hornof, K. Kaarniranta, P. Johansson, A. Urtti, Corneal epithelium as a platform for secretion of transgene products after transfection with liposomal gene eyedrops, J. Gene Med. 9 (2007) 208–216.
[60] E. Mannermaa, S. Rönkkö, M. Ruponen, M. Reinisalo, A. Urtti, Long-lasting secretion of transgene product from differentiated and filter-grown retinal pigment epithelial cells after nonviral gene transfer, Curr. Eye Res. 30 (2005) 345–353.
[61] M. Verdugo, J. Ray, Age-related increase in activity of specific lysosomal enzymes in the human retinal pigment epithelium, Exp. Eye Res. 65 (1997) 231–240, http://dx.doi.org/10.1006/exer.1997.0325.
[62] S. Deshayes, M.C. Morris, G. Divita, F. Heitz, Cell-penetrating peptides: tools for intracellular delivery of therapeutics, Cell. Mol. Life Sci. 62 (2005) 1839–1849.
[63] E. Vivès, J. Schmidt, A. Pèlegrin, Cell-penetrating and cell-targeting peptides in drug delivery, Biochim. Biophys. Acta 1786 (2008) 126–138.
[64] F. Heitz, M.C. Morris, G. Divita, Twenty years of cell-penetrating peptides: from molecular mechanisms to therapeutics, Br. J. Pharmacol. 157 (2009) 195–206.
[65] S.B. Fonseca, M.P. Pereira, S.O. Kelley, Recent advances in the use of cell-penetrating peptides for medical and biological applications, Adv. Drug Deliv. Rev. 61 (2009) 953–964.
[66] W.L. Munyendo, H. Lv, H. Benza-Ingoula, L.D. Baraza, J. Zhou, Cell penetrating peptides in the delivery of biopharmaceuticals, Biomolecules 2 (2012) 187–202.
[67] A. Moshnikova, V. Moshnikova, O.A. Andreev, Y.K. Reshetnyak, Antiproliferative effect of pHLIP-amanitin, Biochemistry 52 (2013) 1171–1178, http://dx.doi.org/10.1021/bi301647y.
[68] K.A. Whitehead, R. Langer, D.G. Anderson, Knocking down barriers: advances in siRNA delivery, Nat. Rev. Drug Discov. 8 (2009) 129–138.
[69] S.K. Soininen, K.-S. Vellonen, A.T. Heikkinen, S. Auriola, V.-P. Ranta, A. Urtti, M. Ruponen, Intracellular PK/PD relationships of free and liposomal doxorubicin: quantitative analyses and PK/PD modeling, Mol. Pharm. 13 (2016) 1358–1365.
[70] M. Egli, S. Sarkhel, Lone Pair—Aromatic Interactions: To Stabilize or Not to Stabilize, Acc. Chem. Res. 40 (2007) 197–205.
[71] S. Sarkhel, G.R. Desiraju, N—H…O, O—H…O, and C—H…O hydrogen bonds in protein-ligand complexes: strong and weak interactions in molecular recognition, Proteins 54 (2004) 247–259.
[72] M.J. Plevin, D.L. Bryce, J. Boisbouvier, Direct detection of CH/pi interactions in proteins, Nat. Chem. 2 (2010) 466–471.
[73] G. Desiraju, T. Steiner, The Weak Hydrogen Bond, Oxford University Press, 2001.
[74] E.M. del Amo, A.-K. Rimpelä, E. Heikkinen, O.K. Kari, E. Ramsay, T. Lajunen, M. Schmitt, L. Pelkonen, M. Bhattacharya, D. Richardson, A. Subrizi, T. Turunen, M. Reinisalo, J. Itkonen, E. Toropainen, M. Casteleijn, H. Kidron, M. Antopolsky, K.-S. Vellonen, M. Ruponen, A. Urtti, Pharmacokinetic Aspects of Retinal Drug Delivery, Prog. Retin, Eye Res, 2016http://dx.doi.org/10.1016/j.preteyeres.2016.12.001.
[75] D. Trifunović, B. Arango-Gonzalez, A. Comitato, M. Barth, E.M. del Amo, M. Kulkarni, A. Sahaboglu, S.M. Hauck, A. Urtti, Y. Arsenijevic, M. Ueffing, V. Marigo, F. Paquet-Durand, HDAC inhibition in the *cpfl1* mouse protects degenerating cone photoreceptors *in vivo*, Hum. Mol. Genet. 25 (2016) ddw275, http://dx.doi.org/10.1093/hmg/ddw275.
[76] S.J. Robbie, P. Lundh von Leithner, M. Ju, C.A. Lange, A.G. King, P. Adamson, D. Lee, C. Sychterz, P. Coffey, Y.-S. Ng, J.W. Bainbridge, D.T. Shima, Assessing a novel depot delivery strategy for noninvasive administration of VEGF/PDGF RTK inhibitors for ocular neovascular disease, Invest. Ophthalmol. Vis. Sci. 54 (2013) 1490–1500.
[77] M.T. Marra, P. Khamphavong, P. Wisniecki, H.J. Gukasyan, K. Sueda, Solution formulation development of a VEGF inhibitor for intravitreal injection, AAPS PharmSciTech 12 (2011) 362–371.